AGU PUBLICATIONS

Geophysical Research Letters

RESEARCH LETTER
10.1002/2016GL071066

Key Points:
- Aircraft data validate surface winds from satellite scatterometers in tropical cyclones (TCs)
- Earth-, motion-, and shear-relative analyses support past studies and highlight new TC findings
- Motion (shear) impacts on surface wind structure are directly (inversely) related to TC intensity

Supporting Information:
- Supporting Information S1
- Table S1
- Table S2
- Table S3

Correspondence to:
B. W. Klotz,
bklotz@rsmas.miami.edu

Citation:
Klotz, B. W., and H. Jiang (2016), Global composites of surface wind speeds in tropical cyclones based on a 12 year scatterometer database, *Geophys. Res. Lett.*, *43*, doi:10.1002/2016GL071066.

Received 13 JUN 2016
Accepted 21 SEP 2016
Accepted article online 23 SEP 2016

Global composites of surface wind speeds in tropical cyclones based on a 12 year scatterometer database

Bradley W. Klotz[1,2] and Haiyan Jiang[2]

[1]Cooperative Institute for Marine and Atmospheric Studies, Rosenstiel School of Marine and Atmospheric Science, University of Miami, Coral Gables, Florida, United States, [2]Earth and Environment Department, Florida International University, Miami, Florida, United States

Abstract A 12 year global database of rain-corrected satellite scatterometer surface winds for tropical cyclones (TCs) is used to produce composites of TC surface wind speed distributions relative to vertical wind shear and storm motion directions in each TC-prone basin and various TC intensity stages. These composites corroborate ideas presented in earlier studies, where maxima are located right of motion in the Earth-relative framework. The entire TC surface wind asymmetry is down motion left for all basins and for lower strength TCs after removing the motion vector. Relative to the shear direction, the motion-removed composites indicate that the surface wind asymmetry is located down shear left for the outer region of all TCs, but for the inner-core region it varies from left of shear to down shear right for different basin and TC intensity groups. Quantification of the surface wind asymmetric structure in further stratifications is a necessary next step for this scatterometer data set.

1. Introduction

Surface winds within a tropical cyclone (TC) are significant for determining a TC's destructive potential. Although the maximum tangential wind within an intensifying TC is found above the surface layer [*Smith et al.*, 2009; *Montgomery et al.*, 2009, 2014], a TC's intensity is officially defined by its surface winds. This definition has implications for the effects of storm surge along coastal communities and for determining the need for evacuations. Understanding of the TC surface wind field, especially within the inner core, has improved over the past several decades due to observations from TC-penetrating aircraft [*Aberson et al.*, 2006; *Rogers et al.*, 2013] with instrumentation such as the stepped frequency microwave radiometer (SFMR) [*Uhlhorn et al.*, 2007; *Klotz and Uhlhorn*, 2014] and Global Positioning System (GPS) dropsondes [*Hock and Franklin*, 1999; *Franklin et al.*, 2003]. Contributions from satellite-based instruments, such as QuikSCAT [*Draper and Long*, 2002, 2004; *Hoffman and Leidner*, 2005] and ASCAT [*Figa-Saldaña et al.*, 2002], have enhanced the understanding of surface winds in TCs, especially of extended range features.

While there is a clear necessity for obtaining surface wind observations in TCs, aircraft and satellite platforms both have their limitations, which makes it sometimes difficult to perform climatological studies. Conversely to the numerous precipitation-related composite studies [*Frank and Ritchie*, 1999; *Corbosiero and Molinari*, 2003; *Lonfat et al.*, 2004; *Chen et al.*, 2006; *Cecil*, 2007; *Jiang*, 2012; *Jiang et al.*, 2013; *Zagrodnik and Jiang*, 2014; *Tao and Jiang*, 2015], few studies have examined the surface winds in a composite form, mainly due to fewer observations of surface winds in TCs. Several recent studies have used scatterometer data to evaluate storm size and the causes of variability [*Chavas and Emanuel*, 2010; *Chan and Chan*, 2012, 2015; *Chavas et al.*, 2016], but these articles focus on the outer core of the TC circulation (generally between 150 and 300 km from the TC center). Studies that have provided some examination of the inner core in a composite sense [*Ueno and Kunii*, 2009; *Ueno and Bessho*, 2011; *Uhlhorn et al.*, 2014, U14] are either limited by the amount of data used, data quality, or region of interest. Because of these constraints, it is difficult to diagnose how the inner core and outer region of the TC surface wind field changes when stratified by TC intensity, storm motion, or vertical wind shear.

In light of this lack of understanding a 12 year, global data set of rain-corrected scatterometer surface wind speeds is utilized in an effort to provide a basin-dependent, global climatology of surface wind speeds in TCs. Section 2 summarizes the data and methodology used, and section 3 shows the initial results of composite wind speed fields compared to theoretical results with a focus on each TC-prone basin. Section 4

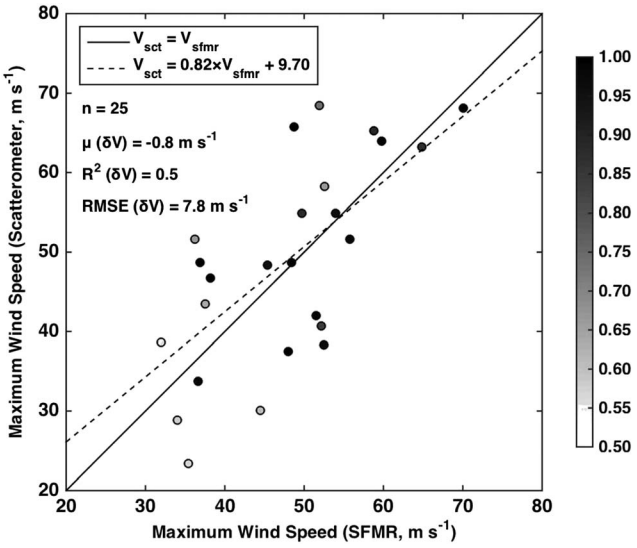

Figure 1. Markers indicate the coincident pairs (±5 h) of maximum surface wind speed (m s^{-1}) from SFMR and scatterometer. Shading of the markers indicates the weight applied to the scatterometer swath. A weighted, linear regression fit (dashed line) is compared to the perfect fit (solid line), with the fit equation provided in the legend. The symbol δV indicates that the printed quantity is based on the difference between the paired maximum wind speeds.

presents the shear- and motion-relative change in wind field structure as a function of TC intensity, and section 5 presents the conclusions and next steps.

2. Data and Methodology

Aircraft-based platforms are useful for observing hurricane force wind speeds, but they are unable to provide a snapshot of the full TC wind field. The satellite-based scatterometer is conversely but advantageously equipped to observe a two-dimensional TC surface wind field at a particular time with somewhat reduced horizontal resolution (12.5 km or ~ 1/8°) [*Brennan et al.*, 2009]. The data used herein are obtained from QuikSCAT and Oceansat-2 (OSCAT) scatterometers, which are available through NASA's Jet Propulsion Laboratory (JPL) Tropical Cyclone Information System archive (TCIS) [*Hristova-Veleva et al.*, 2013]. Scatterometer overpasses are provided for individual cases within each TC basin between years 2000 and 2011. Abbreviations for each basin or their combinations are used throughout the text and include North Atlantic (NATL), Eastern North Pacific and Central Pacific (EPCP), Northwest Pacific (WPAC), and Southern Indian and Southwest Pacific (SHEM). Because scatterometer swaths may miss portions of a TC, a weighting factor between 0 and 1 is calculated from a combination of percentage of TC coverage in the swath within 1.25° (~125 km) and 2.5° (~250 km) of the storm center. To reduce anomalous results, only cases with weights > 0.7 are used herein. Over 75% of the cases have a weight > 0.9, which indicates that TC coverage will not hinder or provide additional uncertainties to the wind speed analysis.

Due to rain contamination of wind speed and direction, a neural network (NN) correction is applied to the scatterometer winds [*Stiles et al.*, 2014]. Uncertainty in the directional ambiguities remains after the correction; however, this directional issue is being addressed in a current study [*Foster et al.*, 2016] that utilizes an inflow angle model [*Zhang and Uhlhorn*, 2012] to provide a basis for correcting the wind direction. Often these ambiguity issues are not widespread across a swath but tend to be more localized [*Stiles et al.*, 2014; J. Zhang, personal communication]. The applied NN correction allows for accurate assessments of wind speeds regardless of storm strength (with slightly higher uncertainty at wind speeds $>$ 55–60 m s^{-1}).

Because of the lower horizontal resolution of the scatterometer compared to aircraft observations from SFMR [*Uhlhorn et al.*, 2007; *Klotz and Uhlhorn*, 2014], it might be assumed that scatterometer data are limited in their ability to provide assessments of TC surface structures. This question stems from the notion that the scatterometer cannot resolve an accurate radius of maximum winds (RMWs) and provide valid radial profiles. While the RMW is generally 10–15 km larger than determined from SFMR (not shown), scatterometer wind speeds (with NN correction) compare reasonably well to those from the SFMR. Figure 1 provides a scatterplot and weighted linear regression fit for the maximum wind speed observed from the SFMR and from the scatterometer. Coincident times are determined as ±5 h of the initial SFMR time. Although the root-mean-square error (RMSE) is higher than desired, it is clear that scatterometers can produce maximum wind values on par with operational aircraft data. It should also be noted that when comparing cases that have larger RMW (the lower limit of the scatterometer is ~25 km), the fit is less variable and the RMSE drops to ~4.5 m s^{-1}. Therefore, larger storms will provide a better opportunity to observe the maximum surface wind. To present the wind fields in composite form, the scatterometer winds are placed on a polar grid with radius normalized by the

RMW, where the TC center is determined subjectively based on a combination of wind direction, backscatter coefficient, and best track location. One might question normalizing the radial grid by the RMW, but in order to truly understand the inner-core structure, normalizing allows for a better evaluation in the composite framework than if using a standard radial grid. Figure S1 in the supporting information provides supporting evidence that an ample number of cases exist at extended radii to have a reasonable representation of the wind field in this framework.

The best track locations and official storm characteristics are obtained from HURDAT2 [*Jarvinen et al*., 1984; *Landsea and Franklin*, 2013] and Joint Typhoon Warning Center reports. Generally, the wind direction provides an adequate center estimate (see note above related to directional ambiguity), but the backscatter coefficient provides verification of the wind-derived center. For reference, Table S1 lists the number of scatterometer passes for each basin based on TC intensity as well as some other key storm and environmental characteristics. Two-dimensional fields are then rotated based on the motion heading by the best track sources mentioned previously or for shear heading provided in the Statistical Hurricane Intensity Prediction Scheme (SHIPS) database [*DeMaria and Kaplan*, 1994, 1999].

Shear is calculated for a deep layer (between 850 and 200 hPa), and the vortex has been removed through 500 km radially outward of the TC center. One might argue the representativeness of this deep-layer shear for shallow TCs. A shear profile would provide a better estimate of the shear at different levels [*Elsberry and Jeffries*, 1996], but several studies have shown that strong deep-layer shear negatively impacts the development of weak TCs [*Frank and Ritchie*, 2001; *Heymsfield et al*., 2006]. Evaluation of the shallow-layer shear vector in SHIPS, which arguably still contains impacts from a vortex, provides inconclusive results. For weaker TCs examined by basin, NATL shallow shear vectors differ from the deep-layer shear more in speed than heading, where median differences are 5 m s^{-1} and −8.0°, respectively. The opposite is true for WPAC cases, where median shear headings differ by −28.5° but shear speeds differ by 2.5 m s^{-1}. Based on this analysis, there is not enough evidence to indicate that a shallow shear is more representative than the deep-layer shear in terms of affecting the shallow vortex. Therefore, the deep-layer shear should be an appropriate metric for evaluating the wind shear for tropical depressions and storms. For a more detailed description of the basin characteristics of storm motion, vertical wind shear, and their relationship, please consult Figure S2.

3. Comparison to Theoretical and Observational Studies Using Basin-Dependent Composites

Several theoretical modeling studies [*Shapiro*, 1983, S83; *Kepert*, 2001; *Thomsen et al*., 2015] examined structural properties of TC vortices in regard to boundary layer convergence and upward motion. Despite using different models, they conclude that the maximum total wind speed in the boundary layer is down motion right in an Earth-relative frame. This is consistent with some observational case studies using in situ wind measurements [*Powell*, 1982, Figure 9] and aircraft remote sensing data [U14, Figure 8b]. S83 also showed a down motion left maximum of total wind in a motion-relative frame (after removing the motion vector, his Figure 5b). Subsequent references to motion-relative quadrants are abbreviated in the form DM for down motion or UM for up motion. Addition of "R" or "L" signifies right or left of the motion vector. For example, down-motion right or right-of-motion are denoted as DMR and RM, respectively. Similar abbreviations follow for shear-relative quadrants, where "S" is used instead of "M" (i.e., DS instead of DM).

Using the scatterometer data, it is possible to test these modeling or observational case-based results within each basin and as a function of storm motion and wind shear in a statistical, composite way. In all composites, storm-centered wind speeds are normalized by the maximum of the composite to more easily compare between the various stratifications. In an Earth-relative reference frame (motion vector not removed), shown in Figure 2 (top row) all basins display a nearly 90° right of motion orientation, with a little less than 90° for EPCP storms. Note that SHEM cases have been rotated to a Northern Hemisphere grid by mirroring around the motion or shear direction to account for the Coriolis effect as in *Chen et al*. [2006]. Statistical significance within each composite analysis is computed using a paired Kolmogorov-Smirnov test at each grid point, determining the median p value, and using this p value as an overall estimate of each motion- (or shear-) relative quadrant. Because analysis at extended radii (>4–5 × RMW) in this framework is considered less meaningful [*Chavas et al*., 2016], composite results are only presented to 5 × RMW. Lighter shading in the NATL and SHEM composites indicates regions where statistical significance (95%) is not attained. These

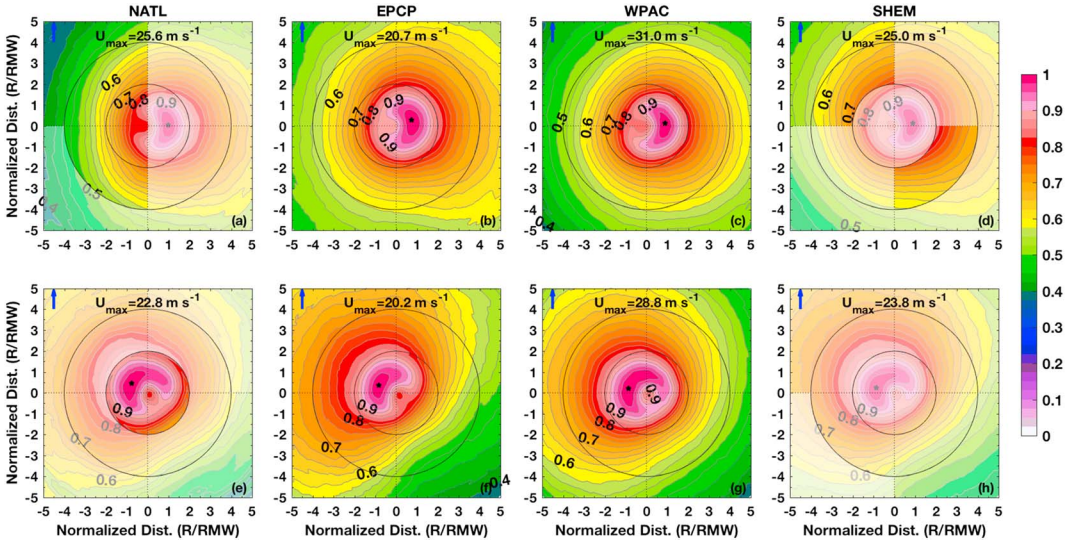

Figure 2. Composite, normalized wind speed analyses are provided for NATL, EPCP, WPAC, and SHEM in a motion-relative reference frame (a–d) with and (e–h) without translation effects, respectively. The storm-centered figures are plotted on a radial polar grid using a normalized radius (R/RMW). Contour lines are plotted in increments of 0.025 normalized units, where a value of 1 is equal to the maximum. The blue arrow is the direction of the motion vector, and the black marker indicates the location of the maximum wind speed. The maximum wind speed value is also indicated on each panel for reference. Black range rings in each panel are plotted at 2x and 4xRMW. Lighter shading indicates areas that do not attain 95% statistical significance when compared to the global composite.

results convey that the global composite (not shown) most closely resembles these two basin composites and that EPCP and WPAC composites deviate significantly from the global composite. The detailed significance values for Figure 2 as well as for other composites presented are provided in Tables S2 and S3. Although the orientation displayed differs from the DMR preference found by the previous studies mentioned above, it is consistent with rather earlier results [*Rossby*, 1948; *Kuo*, 1969; *George and Gray*, 1976; *Jones*, 1977; *Brand et al*., 1981; *Holland*, 1983, 1984; *Chan and Williams*, 1987]. Traditionally, Earth-relative surface wind fields have been approximated as a simple translating axisymmetric vortex with a wave number 1 asymmetry maximized RM.

Motion-relative composites (with motion vector removed) are provided in Figures 2e–2h. All composites are now oriented DML, further confirming that the translation speed has a significant impact on the asymmetry structure of the wind field. Interpretation of statistical significance is similar to Figures 2a–2d. In this framework, S83 indicates that the boundary layer flow is maximized DML, which is consistent with what is found here. Using U14 as an approximate guide, flight level wind maxima are generally 45–60° upwind of the surface maxima at translation speeds comparable to the mean for the scatterometer composites, although the vortex translation has not been removed in their analysis. The SFMR cases in the validation of the scatterometer winds (Figure 1) are used to provide an initial assessment of the conditions with the motion removed. The wave number 1 phase of the maximum surface and flight level wave number 0 + 1 amplitude is calculated and motion is removed following the coefficients in U14's Table 2. Although the sample here is small, the peak flight-level asymmetry approximately occurs near −30° (DML) and the surface phase peaks between −30° and −60° of the flight-level phase. This result provides support for the result shown in Figure 2 where the scatterometer wind maxima are generally LM to DML (−90° to −60° of motion direction).

Figure 3 provides a similar analysis but in a shear-relative reference frame. Previous surface wind speed analyses have shown preference for DSL orientations within smaller samples [*Ueno and Bessho*, 2011, U14]. As seen in Figures 3a–3d, before removing the motion vector, the surface wind asymmetry has a high degree of variability between the basins. In the NATL composite, the shear is generally in the same direction as or to the right of motion (Figure S2) and the wind field is mostly oriented DS. This result is consistent with a DMR to RM orientation as in Figure 2a. The WPAC composite experiences shear that is generally to the left or in the same direction as motion. Figure 3c indicates a DSR maximum wind speed, but the innermost contour is

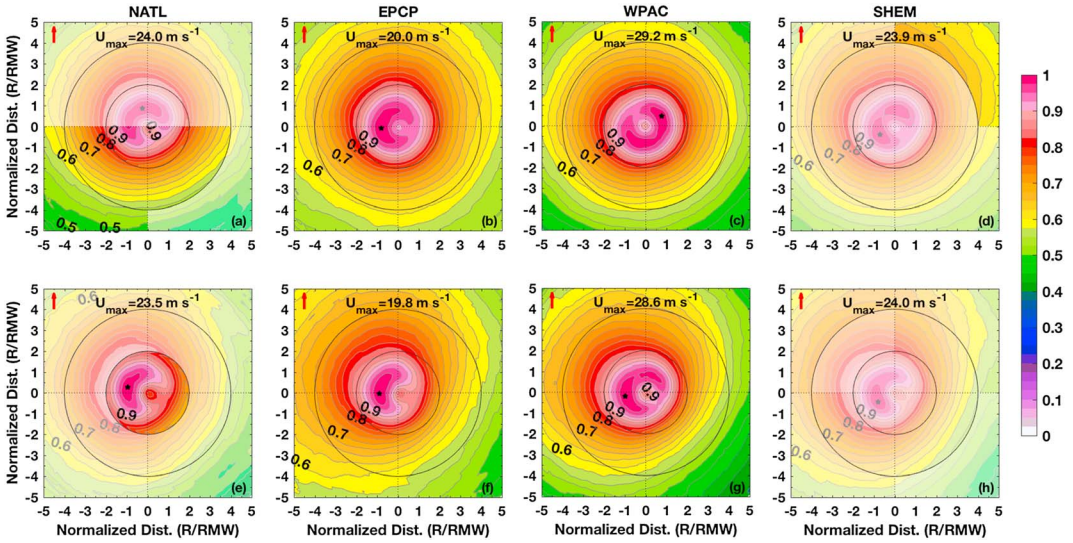

Figure 3. Similar to Figure 2 but for a shear-relative reference frame. The red arrow indicates the shear direction.

rotated USR, which is also consistent with the significant influence from motion from Figure 2c. After removing translation effects, all basin composites show a DSL asymmetry for the midrange (2–4 × RMW) and outer (>4 × RMW) region of the surface wind field For the inner region (<2 × RMW), the asymmetry maximum is mainly LS with some variation either DSL or USL. U14 provides support for this result as well, where they indicate that as shear increases, the surface wave number 1 phase rotates downwind from DS to LS. Because the mean shear values for the basin-specific composites range from 6 to 8 m s^{-1}, the results in Figure 3 are slightly downwind of U14's location. Most of the panels here are statistically significant at 95%. It is encouraging that the analyses developed from the scatterometer overpasses, despite their lack of horizontal resolution, are capable of producing results that agree with previous studies.

4. Wind Shear and Storm Motion Impact Based on TC Intensity

Improvements upon the results of U14 and *Ueno and Bessho* [2011] are accomplished by stratifying storms based on their intensity. Their results are specific for hurricane intensities, while the global scatterometer database contains a substantially large sample at all TC intensities. Rather than belabor the previous section's analysis without removing translation impacts, Figure S3 provides the motion- and shear-relative composites as a function of TC intensity with similar results to those previously mentioned (RM- and variably oriented shear-relative fields). The focus for this section is on these same composites but with motion removed. Figure 4 provides normalized wind speed composites as a function of intensity for motion- and shear-relative reference frames in Figures 4a–4c and Figures 4d–4f, respectively. All panels are statistically significant at 95% through 4–5 × RMW. The middle to outer region of all TC intensity groups and the inner region of nonmajor hurricane cases (tropical storms and Category 1 and 2 hurricanes) display a surface wind asymmetry oriented DML as with the basin composites. Major hurricanes have a DM-oriented maximum in the inner region with rotation DML as radius increases. Due to the presence of moderately strong shear within weak TC's (see Table S1), it is likely that shear is impacting the structure close to the peak winds. As intensity increases and shear decreases, the composites indicate possibly more impact from motion than from shear due to the increased radial extent of the DM signature.

In the shear-relative composites of Figure 4, the outer region of all TC intensity groups and the inner region of tropical depressions and tropical storms display a surface wind asymmetry oriented DSL. However, for the inner region, Category 1 and 2 hurricanes show an USL asymmetry, while the major hurricane group shows a DSR asymmetry. This indicates that the shear likely has a large impact on a TC's middle to outer region for hurricanes but has impacts on the entire wind field of tropical depressions and storms. On the other hand, even after removing the motion vector, the residual motion influence is still strong enough in major hurricanes to rotate the motion and shear-relative structure upwind of the preferred DML and DSL orientations,

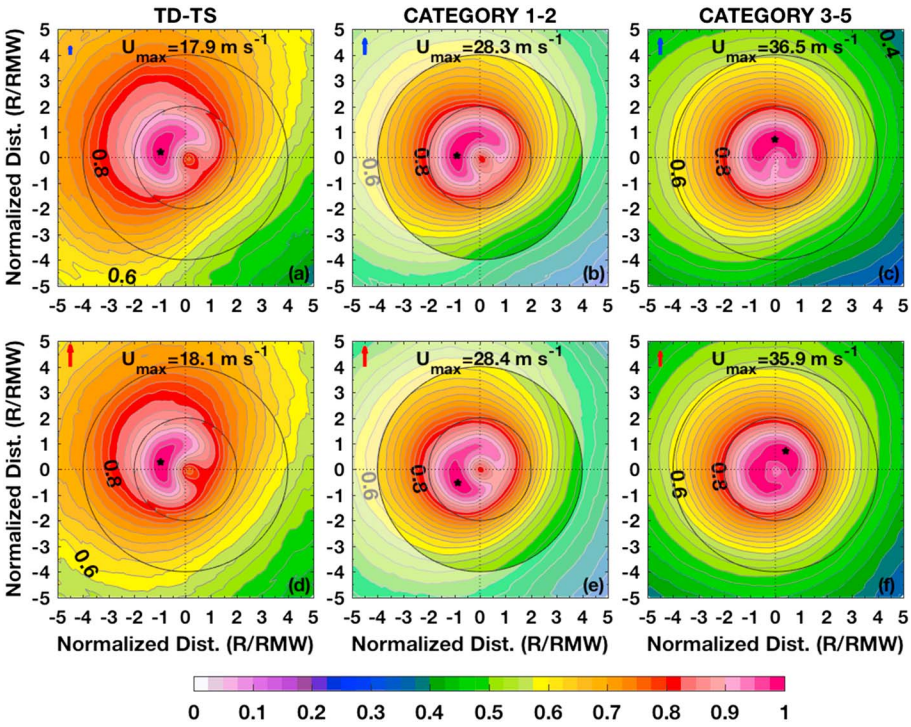

Figure 4. Global composites of normalized wind speed as a function of TC intensity are provided similarly to Figures 2 and 3 for (a, d) tropical depressions and storms, (b, e) nonmajor hurricanes, and (c, f) major hurricanes in storm motion- and shear-relative frameworks (motion vector removed) in Figures 4a–4c and Figures 4d–4f, respectively.

respectively. This result speaks to vortex resiliency to shear and motion residual effects as the intensity increases [*Reasor and Eastin*, 2012; *Reasor et al*., 2013]. U14 suggests a 3–5 m s^{-1} additional contribution of the asymmetry amplitude from shear, but this can be evaluated when quantifying the asymmetry in the future. Additionally, results that compare the full range of storm motion to slow moving cases (not shown, not statistically significant) indicate that Category 1 and 2 hurricane orientations rotate anticyclonically from DML to DM. Tropical storms and major hurricanes are almost unchanged in their motion-relative structure, which suggests that the residual motion effects for weak systems are substantially lower in strength than the shear influence. For strong hurricanes, the opposite relationship may exist, where residual motion factors significantly influence at least the inner region of the TC. It would then be plausible to consider that Categories 1 and 2 hurricanes represent a transition threshold between which motion and shear impacts are both influencing the vortex in similar capacities. Note that friction velocities in TCs increase with increasing wind speed up to ~40 m s^{-1}, where they begin to decrease slightly [*Powell*, 1980; *Powell et al*., 2003]. This knowledge supports the hypothesis that as shear decreases with increasing intensity and friction velocity is maximized near Categories 1 and 2 strength, the primary impact on structure might be alternating from shear to residual motion factors. Also considering that *Chan and Chan* [2015] determined a threshold latitude at which storm size maximizes, changes with preferred motion and shear heading and speed with increasing latitude (see Figure S4) likely contribute to some of the variation in the observed surface wind structure as well. This hypothesis is beyond the scope of the current study but is reserved for future consideration.

5. Conclusions and Next Steps

TC-centered composite wind speed fields were developed based on a large database of scatterometer surface winds that were able to reproduce results that confirm our current understanding of motion-relative and shear-relative asymmetric structure. In the Earth-relative framework before removing the motion vector, the motion impact is dominant over the shear impact, producing a RM asymmetry that is consistent with many earlier studies. The basin-specific composites provide insight into the motion-relative asymmetric field as described in previous theoretical studies by S83, *Kepert* [2001], and *Thomsen et al*. [2015]

and observational studies by *Ueno and Bessho* [2011] and U14. After removing the motion vector, the residual motion effects along with shear effects produce a DML asymmetry of surface wind except for the inner region of major hurricanes. Based on the Earth-relative results, the shear impact on surface wind asymmetry of TCs is secondary to the motion impact, which is the opposite as for the precipitation/convection asymmetry. Many previous studies have shown a shear-dominant precipitation asymmetry with a DSL orientation [e.g., *Chen et al*., 2006]. The shear impact on surface wind appears only after removing the motion vector. The motion-removed composites in the shear-relative framework show a DSL surface wind asymmetry for the outer region of all TCs and the inner region of tropical depressions and storms. For the inner region, the shear-relative asymmetry changes in orientation as a function of intensity. Therefore, the authors hypothesize a possible transition intensity range within nonmajor hurricanes at which motion and shear are similar in their influence on a vortex. Deviations from these structures are possible depending on the shear strength, and shear's relationship to motion plays a crucial role in determining variation of the asymmetric structure. These factors are necessary to consider when quantifying the asymmetric structure.

Based on these results, a set of next steps include assessment and quantification of the low wave number asymmetric surface wind structure as it relates to wind shear and storm motion and the difference between their direction and strength. Separating the relative impacts of shear and motion from the overall composite should be revealing in regard to the results presented in this study. Additionally, intensity change impacts the asymmetric structure in the precipitation/convective components of TCs and is expected to have an impact on the wind component as well. Examining the surface structure based a set of intensity change stratifications will be an important piece to this puzzle as results from future analyses could be connected with results obtained from precipitation studies [*Zagrodnik and Jiang*, 2014; *Tao and Jiang*, 2015].

Acknowledgments

Support for this study was provided by NASA New Investigator Program (NIP) award NNX10AG55G and NASA Hurricane Science Research Program (HSRP) grant NNX10AG34G under the direction of Ramesh Kakar. The scatterometer data were provided by NASA JPL through their TCIS archive (tropicalcyclone.jpl.nasa.gov or ftp://mwsci.jpl.nasa.gov/). SHIPS and HURDAT2 (best track) data are available through CIRA (rammb.cira.colostate.edu/research/tropical_cyclones/ships) and the National Hurricane Center (nhc.noaa.gov/data) and Joint Typhoon Warning Center (usno.navy.mil/NOOC/nmfc-ph/RSS/jtwc/best_tracks), respectively. Comments provided by internal reviewers at NOAA's Hurricane Research Division as well as comments by John Knaff (NOAA) significantly aided the quality of this presented work.

References

Aberson, S. D., M. L. Black, R. A. Black, J. J. Cione, C. W. Landsea, F. D. Marks, and R. W. Burpee (2006), Thirty years of tropical cyclone research with the NOAA P-3 aircraft, *Bull. Am. Meteorol. Soc.*, *87*, 1039–1055, doi:10.1175/BAMS-87-8-1039.

Brand, S., C. A. Buenafe, and H. D. Hamilton (1981), Comparison of tropical cyclone motion and environmental steering, *Mon. Weather Rev.*, *109*, 908–909, doi:10.1175/1520-0493(1981)109<0908:COTCMA>2.0.CO;2.

Brennan, M. J., C. C. Hennon, and R. D. Knabb (2009), The operational use of QuikSCAT ocean surface vector winds at the National Hurricane Center, *Weather Forecasting*, *24*, 621–645, doi:10.1175/2008WAF2222188.1.

Cecil, D. J. (2007), Satellite-derived rain rates in vertically sheared tropical cyclones, *Geophys. Res. Lett.*, *34*, L02811, doi:10.1029/2006GL027942.

Chan, J. C.-L., and R. T. Williams (1987), Analytical and numerical studies of the beta-effect in tropical cyclone motion. Part I: Zero mean flow, *J. Atmos. Sci.*, *44*, 1257–1265, doi:10.1175/1520-0469(1987)044<1257:AANSOT>2.0.CO;2.

Chan, K. T.-F., and J. C.-L. Chan (2012), Size and strength of tropical cyclones as inferred from QuikSCAT data, *Mon. Weather Rev.*, *140*, 811–824, doi:10.1175/MWR-D-10-05062.1.

Chan, K. T.-F., and J. C.-L. Chan (2015), Global climatology of tropical cyclone size as inferred from QuikSCAT data, *Int. J. Climatol.*, *35*, 4843–4848, doi:10.1002/joc.4307.

Chavas, D. R., and K. A. Emanuel (2010), A QuikSCAT climatology of tropical cyclone size, *Geophys. Res. Lett.*, *37*, L18816, doi:10.1029/2010GL044558.

Chavas, D. R., N. Lin, W. Dong, and Y. Lin (2016), Observed tropical cyclone size revisited, *J. Clim.*, *29*, 2923–2939, doi:10.1175/JCLI-D-15-0731.1.

Chen, S. S., J. A. Knaff, and F. D. Marks Jr. (2006), Effects of vertical wind shear and storm motion on tropical cyclone rainfall asymmetries deduced from TRMM, *Mon. Weather Rev.*, *134*, 3190–3208, doi:10.1175/MWR3245.1.

Corbosiero, K. L., and J. Molinari (2003), The relationship between storm motion, vertical wind shear, and convective asymmetries in tropical cyclones, *J. Atmos. Sci.*, *60*, 366–376, doi:10.1175/1520-0469(2003)060<0366:TRBSMV>2.0.CO;2.

DeMaria, M., and J. Kaplan (1994), A Statistical Hurricane Intensity Prediction Scheme (SHIPS) for the Atlantic basin, *Weather Forecasting*, *9*, 209–220, doi:10.1175/1520-0434(1994)009<0209:ASHIPS>2.0.CO;2.

DeMaria, M., and J. Kaplan (1999), An updated Statistical Hurricane Intensity Prediction Scheme (SHIPS) for the Atlantic and Eastern North Pacific basins, *Weather Forecasting*, *14*, 326–337, doi:10.1175/1520-0434(1999)014<0326:AUSHIP>2.0.CO;2.

Draper, D. W., and D. G. Long (2002), An assessment of SeaWinds on QuikSCAT wind retrieval, *J. Geophys. Res.*, *107*(C12), 3212, doi:10.1029/2002JC001330.

Draper, D. W., and D. G. Long (2004), Simultaneous wind and rain retrieval using SeaWinds data, *IEEE Trans. Geosci. Remote Sens.*, *42*, 1411–1423, doi:10.1109/TGRS.2004.830169.

Elsberry, R. L., and R. A. Jeffries (1996), Vertical wind shear influences on tropical cyclone formation and intensification during TCM-92 and TCM-93, *Mon. Weather Rev.*, *124*, 1374–1387, doi:10.1175/1520-0493(1996)124<1374:VWSIOT>2.0.CO;2.

Figa-Saldaña, J., J. J. W. Wilson, E. Attema, R. Gelsthorpe, M. R. Drinkwater, and A. Stoffelen (2002), The advanced scatterometer (ASCAT) on the meteorological operational (MetOp) platform: A follow on for European wind scatterometers, *Can. J. Remote Sens.*, *28*, 404–412, doi:10.5589/m02-035.

Foster, R. C., J. Zhang, and P. Black (2016), Estimates of tropical cyclone surface wind inflow from satellite scatterometers, *32nd AMS Conf. on Hurricanes and Tropical Meteorology*, San Juan, Puerto Rico, 11C.5, Preprints.

Frank, W. M., and E. A. Ritchie (1999), Effects of environmental flow upon tropical cyclone structure, *Mon. Weather Rev.*, *127*, 2044–2061, doi:10.1175/1520-0493(1999)127<2044:AEOEFUT>2.0.CO;2.

Frank, W. M., and E. A. Ritchie (2001), Effects of vertical wind shear on the intensity and structure of numerically simulated hurricanes, *Mon. Weather Rev.*, *129*, 2249–2269, doi:10.1175/1520-0493(2001)129<2249:AEOVWSO>2.0.CO%3B2.

Franklin, J. L., M. L. Black, and K. Valde (2003), GPS dropwindsonde wind profiles in hurricanes and their operational implications, *Weather Forecasting*, *18*, 32–44, doi:10.1175/1520-0434(2003)018<0032:AGDWPIH>2.0.CO;2.

George, J. E., and W. M. Gray (1976), Tropical cyclone motion and surrounding parameter relationships, *J. Appl. Meteorol.*, *15*, 1252–1264, doi:10.1175/1520-0450(1976)015<1252:ATCMASP>2.0.CO;2.

Heymsfield, G. M., J. Simpson, J. Halverson, L. Tian, E. Ritchie, and J. Molinari (2006), Structure of highly sheared Tropical Storm Chantal during CAMEX-4, *J. Atmos. Sci.*, *63*, 268–287, doi:10.1175/JAS3602.1.

Hock, T. F., and J. L. Franklin (1999), The NCAR GPS dropwindsonde, *Bull. Am. Meteorol. Soc.*, *80*, 407–420, doi:10.1175/1520-0477(1999)080<0407:ATNGD>2.0.CO;2.

Hoffman, R. N., and S. M. Leidner (2005), An introduction to the near–real–time QuikSCAT data, *Weather Forecasting*, *20*, 476–493, doi:10.1175/WAF841.1.

Holland, G. J. (1983), Tropical cyclone motion: Environmental interaction plus a beta effect, *J. Atmos. Sci.*, *40*, 328–342, doi:10.1175/1520-0469(1983)040<0328:ATCMEIP>2.0.CO;2.

Holland, G. J. (1984), Tropical cyclone motion: A comparison of theory and observation, *J. Atmos. Sci.*, *41*, 68–75, doi:10.1175/1520-0469(1984)041<0068:ATCMACO>2.0.CO;2.

Hristova-Veleva, S. M., et al. (2013), Revealing the winds under the rain. Part I: Passive microwave rain retrievals using a new observation-based parameterization of subsatellite rain variability and intensity—algorithm description, *J. Appl. Meteorol. Climatol.*, *52*, 2828–2848, doi:10.1175/JAMC-D-12-0237.1.

Jarvinen, B. R., C. J. Neumann, and M. A. S. Davis (1984), A tropical cyclone data tape for the North Atlantic Basin, 1886–1983: Contents, limitations, and uses. NOAA Tech. Memo. 22, NWS/NHC, Miami, FL, 21 pp.

Jiang, H. (2012), The relationship between tropical cyclone intensity change and the strength of inner-core convection, *Mon. Weather Rev.*, *140*, 1164–1176, doi:10.1175/MWR-D-11-00134.1.

Jiang, H., E. M. Ramirez, and D. J. Cecil (2013), Convective and rainfall properties of tropical cyclone inner cores and rainbands from 11 Years of TRMM data, *Mon. Weather Rev.*, *141*, 431–450, doi:10.1175/MWR-D-11-00360.1.

Jones, R. W. (1977), Vortex motion in a tropical cyclone model, *J. Atmos. Sci.*, *34*, 1518–1527, doi:10.1175/1520-0469(1977)034<1518:AVMIATC>2.0.CO;2.

Kepert, J. (2001), The dynamics of boundary layer jets within the tropical cyclone core. Part I: Linear theory, *J. Atmos. Sci.*, *58*, 2469–2484, doi:10.1175/1520-0469(2001)058<2469:ATDOBLJ>2.0.CO;2.

Klotz, B. W., and E. W. Uhlhorn (2014), Improved stepped frequency microwave radiometer tropical cyclone surface winds in heavy precipitation, *J. Atmos. Oceanic Technol.*, *31*, 2392–2408, doi:10.1175/JTECH-D-14-00028.1.

Kuo, H.-L. (1969), Motions of vortices and circulating cylinder in shear flow with friction, *J. Atmos. Sci.*, *26*, 390–398, doi:10.1175/1520-0469(1969)026<0390:AMOVACC>2.0.CO;2.

Landsea, C., and J. Franklin (2013), Atlantic hurricane database uncertainty and presentation of a new database format, *Mon. Weather Rev.*, *141*, 3576–3592, doi:10.1175/MWR-D-12-00254.1.

Lonfat, M., F. D. Marks Jr., and S. S. Chen (2004), Precipitation distribution in tropical cyclones using the Tropical Rainfall Measuring Mission (TRMM) microwave imager: A global perspective, *Mon. Weather Rev.*, *132*, 1645–1660, doi:10.1175/1520-0493(2004)132<1645:APDITCU>2.0.CO;2.

Montgomery, M. T., S. V. Nguyen, R. K. Smith, and J. Persing (2009), Do tropical cyclones intensify by WISHE?, *Q. J. R. Meteorol. Soc.*, *135*, 1697–1714, doi:10.1002/qj.459.

Montgomery, M. T., J. A. Zhang, and R. K. Smith (2014), An analysis of the observed low-level structure of rapidly intensifying and mature hurricane Earl (2010), *Q. J. R. Meteorol. Soc.*, *140*, 2132–2146, doi:10.1002/qj.2283.

Powell, M. D. (1980), Evaluations of diagnostic marine boundary-layer models applied to hurricanes, *Mon. Weather Rev.*, *108*, 757–766, doi:10.1175/1520-0493(1980)108<0757:EODMBL>2.0.CO;2.

Powell, M. D. (1982), The transition of the Hurricane Frederic boundary-layer wind field from the open Gulf of Mexico to landfall, *Mon. Weather Rev.*, *110*, 1912–1932, doi:10.1175/1520-0493(1982)110<1912:TTOTHF>2.0.CO;2.

Powell, M. D., P. J. Vickery, and T. Reinhold (2003), Reduced drag coefficient for high wind speeds in tropical cyclones, *Nature*, *422*, 279–283, doi:10.1038/nature01481.

Reasor, P. D., and M. D. Eastin (2012), Rapidly intensifying Hurricane Guillermo (1997), Part II: Resilience in shear, *Mon. Weather Rev.*, *140*, 425–444, doi:10.1175/MWR-D-11-00080.1.

Reasor, P. D., R. Rogers, and S. Lorsolo (2013), Environmental flow impacts on tropical cyclone structure diagnosed from airborne Doppler radar composites, *Mon. Weather Rev.*, *141*, 2949–2969, doi:10.1175/MWR-D-12-00334.1.

Rogers, R. F., et al. (2013), NOAA's hurricane intensity forecasting experiment (IFEX): A progress report, *Bull. Am. Meteorol. Soc.*, *94*, 859–882, doi:10.1175/BAMS-D-12-00089.1.

Rossby, C. G. (1948), On the displacement and intensity changes of atmospheric vortices, *J. Mar. Res.*, *7*, 175–187.

Shapiro, L. J. (1983), The asymmetric boundary layer flow under a translating hurricane, *J. Atmos. Sci.*, *40*, 1984–1998, doi:10.1175/1520-0469(1983)040<1984:ATABLFU>2.0.CO;2.

Smith, R. K., M. T. Montgomery, and S. V. Nguyen (2009), Tropical cyclone spin-up revisited, *Q. J. R. Meteorol. Soc.*, *135*, 1321–1335, doi:10.1002/qj.428.

Stiles, B. W., R. E. Danielson, W. L. Poulsen, M. J. Brennan, S. Hristova-Veleva, T.-P. Shen, and A. G. Fore (2014), Optimized tropical cyclone winds from QuikSCAT: A neural network approach, *IEEE Trans. Geosci. Remote Sens.*, *52*, 7418–7434, doi:10.1109/TGRS.2014.2312333.

Tao, C., and H. Jiang (2015), Distributions of shallow to very deep precipitation/convection in rapidly intensifying tropical cyclones, *J. Clim.*, *28*, 8791–8824, doi:10.1175/JCLI-D-14-00448.1.

Thomsen, G. L., R. K. Smith, and M. T. Montgomery (2015), Tropical cyclone flow asymmetries induced by a uniform flow revisited, *J. Adv. Model. Earth. Syst.*, *5*, 382–405, doi:10.1002/2015MS000477.

Ueno, M., and K. Bessho (2011), A statistical analysis of near-core surface wind asymmetries in typhoons obtained from QuikSCAT data, *J. Meteorol. Soc. Jpn.*, *89*, 225–241, doi:10.2151/jmsj.2011-304.

Ueno, M., and M. Kunii (2009), Some aspects of azimuthal wavenumber-one structure of typhoons represented in the JMA operational mesoscale analyses, *J. Meteorol. Soc. Jpn.*, *87*, 615–633, doi:10.2151/jmsj.87.615.

Uhlhorn, E. W., P. G. Black, J. L. Franklin, M. Goodberlet, J. Carswell, and A. S. Goldstein (2007), Hurricane surface wind measurements from an operational stepped frequency microwave radiometer, *Mon. Weather Rev.*, *135*, 3070–3085, doi:10.1175/MWR3454.1.

Uhlhorn, E. W., B. W. Klotz, T. Vukicevic, P. D. Reasor, and R. F. Rogers (2014), Observed hurricane wind speed asymmetries and relationships to motion and environmental shear, *Mon. Weather Rev.*, *142*, 1290–1311, doi:10.1175/MWR-D-13-00249.1.

Zagrodnik, J. P., and H. Jiang (2014), Rainfall, convection, and latent heating distributions in rapidly intensifying tropical cyclones, *J. Atmos. Sci.*, *71*, 2789–2809, doi:10.1175/JAS-D-13-0314.1.

Zhang, J. A., and E. W. Uhlhorn (2012), Hurricane sea surface inflow angle and an observation-based parametric model, *Mon. Weather Rev.*, *140*, 3587–3605, doi:10.1175/MWR-D-11-00339.1.